From Ph.D. thesis
Author: Dodla V. Ramana Reddy
Title of thesis: Collective Dynamics of delay coupled oscillators
Work done at: Institute for Plasma Research, Bhat, Gandhinagar, India.
Degree granting university: Gujarat University, Ahmedabad, India.
Year of degree: 2002
Thesis advisor: Abhijit Sen, Institute for Plasma Research.

Chapter 5

Experimental Study of Delay Effects on Coupled Limit Cycle Oscillators

"There is nothing like first-hand evidence."[1]

[1]Sherlock Holmes in *A Study in Scarlet* by Sir Arthur Conan Doyle

5.1 Introduction

To complement and support our theoretical and numerical investigations of the effects of time delay on the collective behavior of coupled limit cycle oscillators we have also carried out a set of experimental studies in this direction and report the experimental results in this Chapter. As can be seen from the earlier chapters, time delay has a variety of effects on the collective dynamics of coupled oscillators. These include stabilization of the origin (leading to amplitude death), creation of multiple frequency states, and suppression of the collective frequency. These characteristic effects can be seen in systems as simple as two coupled oscillators or often in a single feedback driven oscillator. To keep the experimental setup simple we have chosen to limit ourselves to a system consisting of just two identical and time delay coupled limit cycle oscillators. As shown in Chapter 2 this system shows a surprising theoretical result, namely amplitude death with zero frequency dispersion among the oscillators. This important theoretical finding has not been demonstrated experimentally so far and therefore forms a major motivation for our experimental studies.

Our experimental system consists of nonlinear electronic circuits constructed to produce coherent limit cycle states in the single or coupled mode. A variable digital delay line allows us to scan a range of parameter space to verify the nature of the bifurcation curves and to probe the regions of "death islands". The results confirm not only the existence of such regions for identical oscillators but also demonstrate the existence of multiple frequency states, time delay dependent frequency suppression and the simultaneous presence of in-phase and out-of-phase states. The experimental findings are compared with results obtained from approximate theoretical models of the nonlinear circuits and the agreement is found to be very good.

Although a vast literature exists on the use of electronic circuits to experimentally simulate the dynamics of nonlinear systems, we would like to mention here the work of Brailove and Linsay[1] which is one of the earliest in the area of exploring the collective dynamics of coupled oscillators. Their experiments used a system of a large number of (as many as 15) electronically constructed relaxation oscillators to study phase locking between them. For this they utilized a phase-repelling mean field coupling and did not include any time delay in the coupling. Their system which can be theoretically represented as just a set of simple phase coupled oscillators is not capable of exhibiting phenomena like amplitude death. Our system has been designed to observe the collective death state and to study the influence of time delay on it. Our electronic system also closely mimics many real life experimental systems. In particular we have chosen the frequency range

of the oscillators to be such as to be in the domain of the oscillatory behavior of coupled chemical reactors, the rhythmical behavior of pace maker cells in the human heart, or the time duration of flashing of fire flies. The typical time periods in these systems are in the range of a few cycles per second to about a millisecond. Some of the results presented in this Chapter are for frequencies of 100 cycles/sec. We have also worked with frequencies as low as 30 cycles/sec and the system is capable of going to even lower frequencies.

The Chapter is organized as follows. Before getting on to the actual experimental results we discuss in some detail our design philosophy and the electronic sub-components of the basic nonlinear circuit in Section 5.2. In particular the construction of the nonlinear resistance element is discussed and its experimental characteristics presented. This section also describes the time delay element. Section 5.3 is devoted to the experimental study of a single nonlinear circuit with a time delayed linear feedback element. The results are compared to the solution of a suitable mathematical model of the circuit. Section 5.4 addresses the main topic of our experimental study, namely, the dynamics of two coupled nonlinear circuits with time delayed linear coupling. The experimental findings on death of oscillations, the existence of multiple frequencies, the suppression of these frequencies with time delay, etc. are presented and compared to appropriate model theoretical results. The Chapter concludes in Section 5.5 with a summary of the results and a discussion on possible sources of experimental errors.

5.2 Nonlinear component and active inductance

In building a limit cycle oscillator model electronically, one can opt for any of a variety of oscillator circuits. However, one of the simplest and perhaps the easiest to understand analytically is an LCR circuit with a nonlinear resistive element. Several different versions of such circuits have been extensively used in experimental simulation of low dimensional nonlinear dynamical models [2, 3, 4, 5, 6, 7]. We therefore adopt such a model. However, since our eventual goal is to use this circuit along with a time delay element, there are certain restrictions that are imposed on the choice of the components. These essentially arise from the operational limits of the delay circuit. We choose to work with low frequencies: frequencies of the order of 100 Hz. To achieve frequencies of this magnitude, the corresponding values of the inductor would be very high: a few tens of Henry. These values are practically impossible to achieve using conventional wire wound inductors. So there is a natural selection of active inductors which use a capacitance and invert it to

make it act like an inductor. In the following sections we first describe the nonlinear resistive element and then the active inductance element.

5.2.1 The negative resistance element

In order to sustain a limit cycle oscillation in an LCR circuit, the desired voltage-current characteristic curves of the nonlinear resistive element are those that display negative resistance around the origin, and positive slopes away from the origin. Such an element can be constructed using a diode and an OP-AMP circuit. The negative resistance in particular can be achieved with a positive and a negative feedback on the latter. This kind of nonlinear elements or the so called 'function generators' are widely used in electronics for a variety of functions [8, 9]. In Fig. 5.1(a) the circuit diagram is depicted for the negative resistance component that we have constructed. Let V_0 be the output voltage of the OP-AMP. It can be expressed as $V_0 = (R_2/R_1 + 1)V$. Now the current that is flowing into the element is given by

$$I = \frac{1}{R_3}\Big[V - \Big(\frac{R_2}{R_1} + 1\Big)V\Big] = \frac{V}{\Big(\frac{-R_1 R_4}{R_2}\Big)}. \tag{5.1}$$

So the impedance of the component seen from the point at which the voltage is applied appears as negative with the value given by

$$Z_N = -\frac{R_1 R_4}{R_2}. \tag{5.2}$$

The negative resistance thus constructed must be grounded at one end as shown. When this is used along with other circuitry, this end must remain grounded. To actually see the operation of the negative resistance, a set of test experiments are carried out to measure its $V - I$ characteristics. The resulting measurements are marked as circles in the plot shown in Fig. 5.1(b). The solid line represents the above formula for Z_N and as can be seen the agreement between the two is excellent.

5.2.2 The nonlinear component

We now have all the essential ingredients to make the nonlinear element, and we know the characteristic response of each of the sub-components. The full nonlinear element we use in the experiment is shown in Fig. 5.2. Similar *function generators*, as they are called, can be found, for example, in [10]. One of the most popular versions of such generators is extensively used in the electronic simulation of dynamical systems; this is the so called *Chua's diode* [5]. Our present construction in the figure consists of two diodes connected

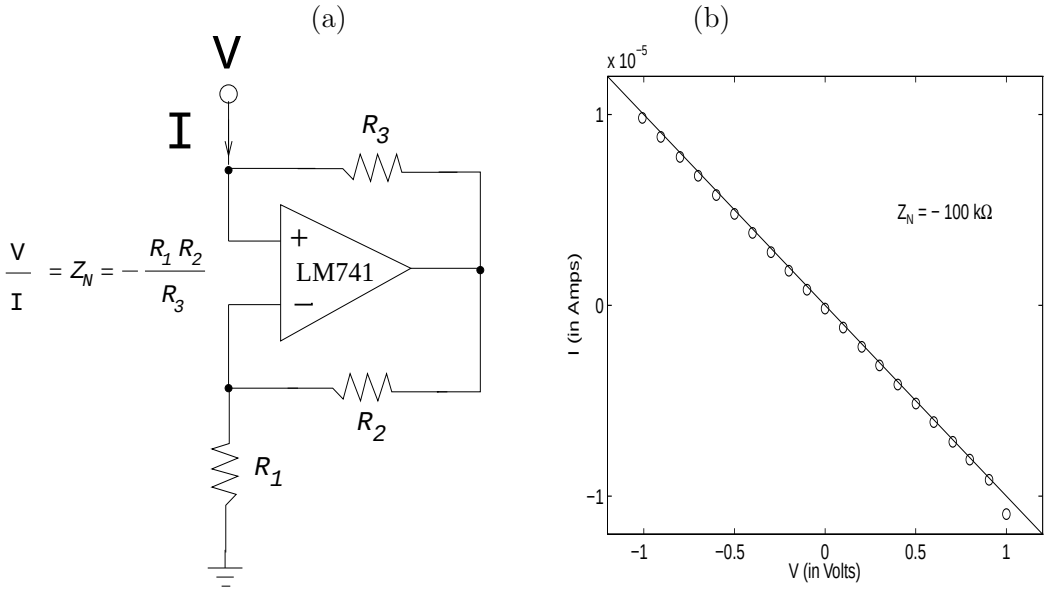

Figure 5.1: Circuit diagram to produce negative resistance and the experimental points (circles) and theoretical curve (line) plotted from the formula (5.2). The parameters are $R_1 = 10$ KΩ, $R_2 = 10$ KΩ and $R_3 = 100$ KΩ which give $Z_N = -100$ KΩ.

back to back in series with a resistance. The negative resistance element is connected in parallel to the diode-resistance branch. From the figure it is clear that an equation can be written between V and I for the entire nonlinear component by noting that $I = I_D + I_N = I_D + V/Z_N$, where we have assumed that I_D and I_N represent respectively the currents flowing through R_D and Z_N. Likewise, the equation of response for a single diode with a series resistance R_D can be expressed as $I = R_D I + \eta V_T \log(I/I_s + 1)$, where at room temperature $\eta V_T = 1/18.336$ and $I_s = 2 \times 10^{-9}$ Amp is the reverse saturation current of the diode. Using the above two relations one can now obtain the following equation for the response of the nonlinear element,

$$V = R_D I - V\frac{R_D}{Z_N} + \eta V_T \ \log\Big(\frac{I}{I_S} - \frac{V}{Z_N I_S} + 1\Big). \tag{5.3}$$

As can be seen from this equation, the negative slope of the resultant curve is largely decided by Z_N. A variation in R_D on the other hand significantly influences the portions pertaining to the positive slopes. The effects of both these parameters can be seen from Fig. 5.3 which are plotted using the above equation. In Fig. 5.4(a), an experimental V-I characteristic is shown (in circles) for the parameters $Z_N = -100$ KΩ, $R_D = 3.5$KΩ by measuring the current flowing through the nonlinear element for a range of applied dc voltages. The solid curve in the figure is plotted by solving the Eq. (5.3). In the construction of Z_N, the values of the resistances are $R_1 = 10$ KΩ, $R_2 = 10$KΩ and

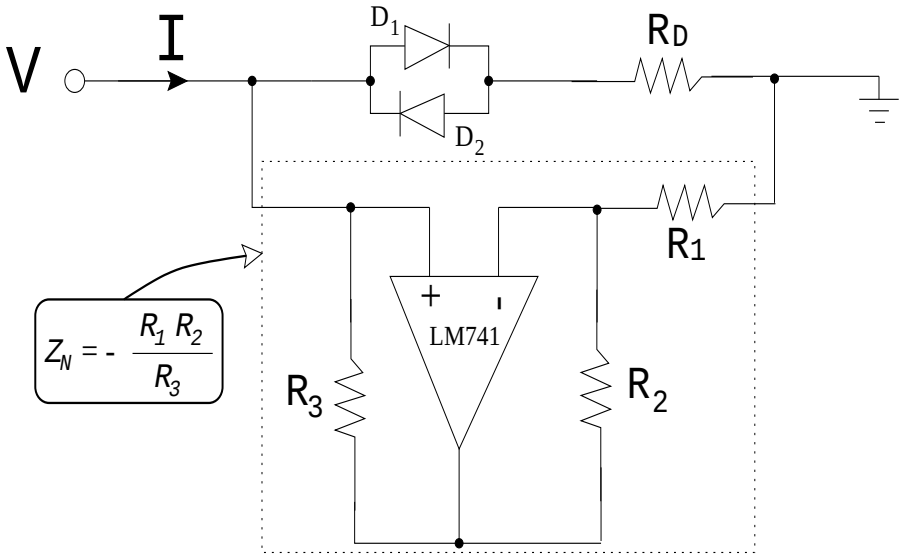

Figure 5.2: The nonlinear element used in the experiment.

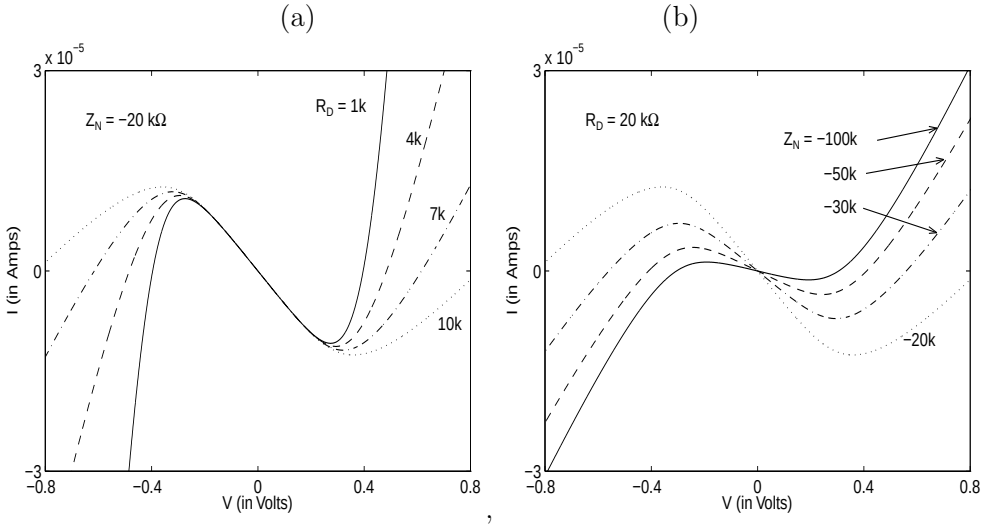

Figure 5.3: A plot of Eq. (5.3) for different values of Z_N and R_D.

$R_3 = 100\text{K}\Omega$. The agreement between the theoretical curve and the experimental points along the negative slope is quite good. There are minor deviations at large values of the operating voltage. However the positive slopes of the curve at large V and that of the experimental points are in correspondence. The main deviation comes in the form of a stretching of the negative resistance region a little more than what is theoretically predicted by Eq. (5.3). Next we approximate the experimental $V - I$ response by using

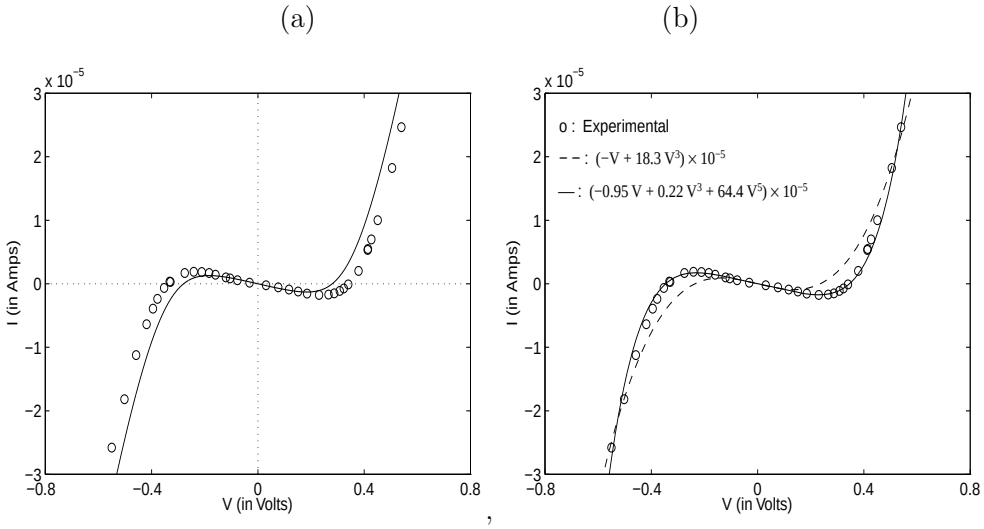

Figure 5.4: (a) Experimentally found V-I characteristics (circles), and the theoretical curve obtained from Eq. (5.3) of the nonlinear resistive element shown in Fig. 5.2. The values chosen are $Z_N = -100$ KΩ and $R_D = 3.5$KΩ. For the theoretical curve the additional parameters chosen are $\eta V_T = 1/18.33$ and $I_s = 2.0 \times 10^{-8}$ Amp. (b) Fit of a polynomial using simplex algorithm for the experimentally found V-I characteristics (circles). The dashed curve is $I = (-V + 18.3V^3) \times 10^{-5}$ and the continuous curve is $I = (-0.95V + 0.22V^3 + 64.4V^5) \times 10^{-5}$.

a simplex algorithm. The results are shown in Fig. 5.4(b). The curve,

$$I = (-0.95V + 0.22V^3 + 64.4V^5) \times 10^{-5} \tag{5.4}$$

approximates the data points quite accurately. We shall use this expression in our later numerical simulations.

We have also checked the response of the nonlinear element to oscillating voltages and found it to be the same. In particular one does not see any hysteresis behavior which would have been expected if one had used a wire wound inductance. In Fig. 5.5 the voltage applied to the nonlinear element and its response, which is proportional to the current passing through the element, are shown from the oscilloscope traces. As is clear the response is quite satisfactory.

5.2.3 Active Inductance

As we discussed in the beginning of this section, we must use an inductor with an inductance of a few Henry, a task that is made possible through the use of 'Generalized Impedance Converters'. The use of these components has become so widely necessary

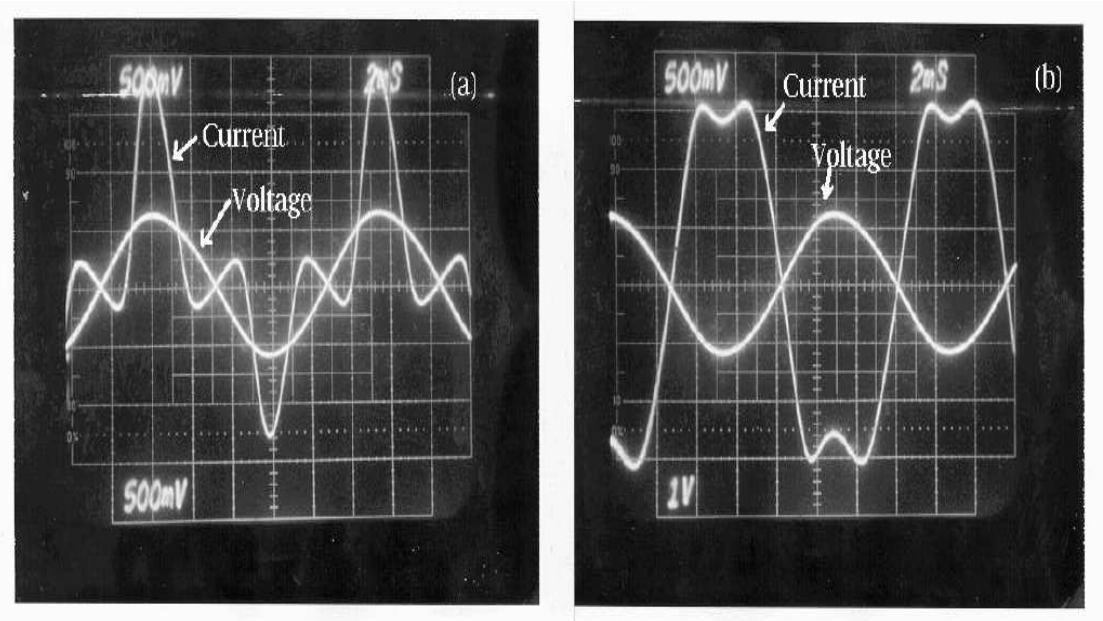

Figure 5.5: The response of the nonlinear element to an applied periodic voltage. (a) The response for $Z_N = -100\text{K}\Omega$. The scale for current is 1 $unit = 0.5/(100 \times 10^3)$ Amp. (b) The response for $Z_N = -10\text{K}\Omega$. The scale for current is 1 $unit = 0.5/(10 \times 10^3)$ Amp. In both the cases, $R_D = 3.5\text{K}\Omega$ and the scale for the voltage is 1 $unit = 0.5V$.

at the present time that they are now available as commercially manufactured IC chips (e.g. AF120 manufactured by National Semiconductors). For our experiment, we have constructed an active inductance element in the following manner.

The general circuit diagram is shown in Fig. 5.6 where two OP-AMPs of type LM741, and five impedances have been put together. By writing down expressions at the nodes between (i) Z_1 and Z_2, and (ii) Z_4 and Z_5, an expression for the voltage applied at A and the current passing through it can be derived. This results in an impedance which is given by

$$Z = \frac{Z_1 Z_3 Z_5}{Z_2 Z_4} \tag{5.5}$$

We set Z_1, Z_3, Z_4 and Z_5 to simple resistances, replace Z_2 by a capacitance and use Z_4 as the variable resistance to achieve the desired inductance value. We make the choice: $Z_1 = R_1 = 10\text{K}\Omega$, $Z_2 = 1/(j\omega C_2)$ with $C_2 = 0.1\mu\,\text{F}$, $Z_3 = 1\text{K}\Omega$, $Z_5 = R_5 = 1\text{K}\Omega$. $Z_4 = R_4$ can be used as a parameter to actually adjust the value of the resultant inductance that

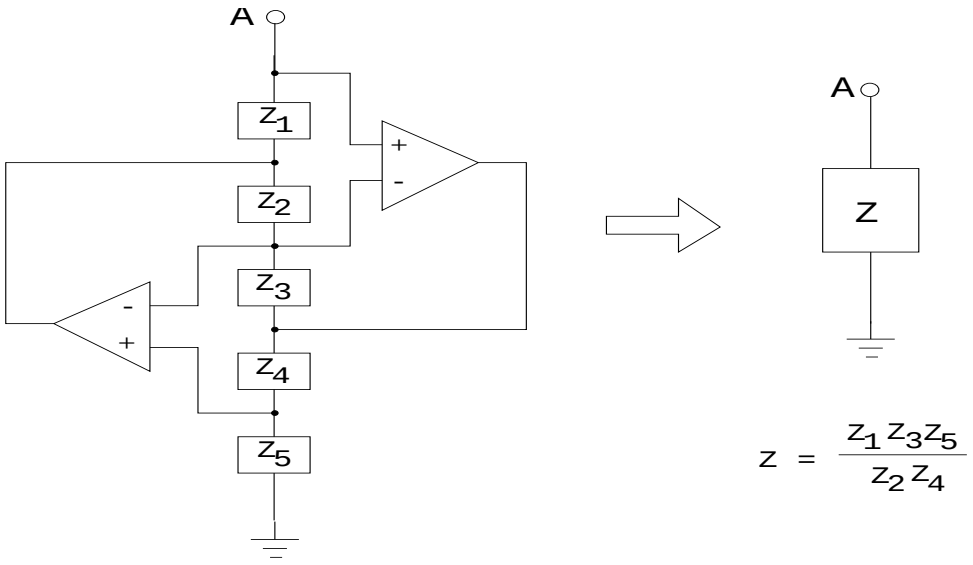

Figure 5.6: Active inductance

is required. For these set of values,

$$Z = j\omega L = \frac{R_1 R_3 R_5}{\left(\frac{1}{j\omega C_2}\right) R_4} = j\omega \frac{10^3}{R_4} \quad \Longrightarrow \quad L = \frac{10^5}{R_4}. \tag{5.6}$$

For example, as this will also be the case in our later experiments, if we chose a capacitance of $C = 0.1\mu$F along with the above L, the resultant angular frequency of the circuit would be

$$\omega = \frac{1}{\sqrt{LC}} = 100\ \sqrt{R_4}. \tag{5.7}$$

5.2.4 Time delay element

The time delay element is assigned the job of sampling the input wave form, storing it and delivering it as an undistorted output after a specified time period. There are in practice two kinds of time delay elements: (i) analog (or passive), and (ii) digital (or active). Analog delay lines are usually long cables (typically looped bundles) often used with discrete directional couplers. The main drawback of such a delay line is the loss of the signal and its enormous size. For delays beyond a few nanoseconds analog systems are extremely uneconomical and often impractical. Digital delay lines on the other hand offer many advantages and are often quite compact. We have adopted such a system for our use. The basic principle involved in the delay element is depicted in Fig. 5.7. The input signal is tapped at a certain rate using an analog to digital converter (ADC) and

Figure 5.7: The process involved in digital delay line.

stored in a random access memory (RAM). The stored bits now can be read using a logical circuit and converted back to an analog signal. Such a procedure causes the least amount of distortions in the signal. However, there are two important points which decide the operational limits of a digital delay line. The first involves the memory of the RAM. The second involves the tapping rate of the signal by ADC. An ADC of high tapping rate (or conversion rate, as it is called) will allow more number of samples per input signal. This essentially decides the maximum frequency of the signal which can be handled by the delay circuit without distortion. Also, the faster the conversion rate, the smaller the time delay step one can reach. A variety of digital delay lines are available commercially. However, due to their predominant use, most of the delay lines are available in pico, nano, and hundreds of micro seconds range. The delay lines that are available in the market for the millisecond and seconds range are optimized for specific applications and are quite expensive. So we acquired a custom made digital delay line for our experiment with delay periods in the millisecond range.

The delay line is made with an ADC0809 (that has a conversion rate of 100μs) and has two input and output channels. So the sampling time is shared between the two channels. This means that for each channel, there can be 5 samples per millisecond. Thus an input signal of 10 millisecond (i.e. 100 cycles/sec.) will have 50 samples picked up by the delay circuit. Higher frequencies will mean less number of samples per cycle and the output will have lots of unfilled 'holes' in the waveform. These discontinuities will be seen by the oscillator components and the results can be unpredictable. So the present delay line is best suited (and that is exactly what it was made for) to deal with smaller frequencies. The lower accessible delay limit is (100 μ s/2) which is 50 μs. To make it suitable for larger frequencies, ADC's of faster conversion rate must be used (e.g., ADC08061 has a conversion rate of 500ns which will have 500samples/ms. This means that we would have had in the present scenario 5000 samples for a signal of 100cycles/sec. The lower accessible limit in such a case would be 0.25 μs.

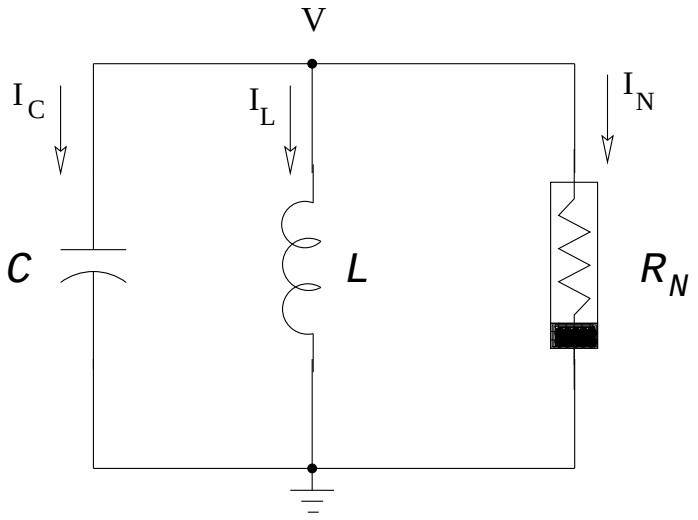

Figure 5.8: Electronic model of a limit cycle oscillator. The fundamental frequency of the oscillator is $\omega = 200\pi$. The values of the components are $C = 0.1\mu$F, $L = 250/\pi^2$. The $V - I$ property of R_N is shown in Fig. 5.4(b).

5.2.5 The Basic Limit Cycle Oscillator Circuit

We have now come to the stage of putting together all the subcomponents we have constructed and described in the previous sections. We are also armed with the experimental properties of each of the components we plan to use. In this section we design the basic limit cycle oscillator and present the experimental waveforms that it produces for various nonlinearities. The limit cycle oscillator is built along the familiar lines of an LCR circuit. In Fig. 5.8 the circuit diagram is given. C is a capacitor. The inductor L is an active inductor as described in Section 5.2.3. The nonlinear resistance R_N has the voltage-current characteristics shown in Fig. 5.4(b). We set the resonant frequency of the LC circuit to 100 Hz. So the angular frequency is $\omega = 200\ \pi$. Hence, $L = 250/\pi^2$. (Using the formula (5.7), $R_4 = 4\pi^2$ which is nearly 40Ω.) We now perform some test runs to check out the experimental waveforms generated by this oscillator circuit. Oscilloscope traces of these waveforms are shown in Fig. 5.9 for different values of the negative resistance Z_N with $R_D = 3.5$KΩ. By varying Z_N, the response of the nonlinear resistance is altered (see Fig. 5.3(b)). As Z_N is decreased, the slope of the curve $I(V)$ increases resulting in a distortion of the periodic orbit. As it increases to a large value, the shape of the wave form is limited or curtailed by the limitations of the biasing voltages (last figure).

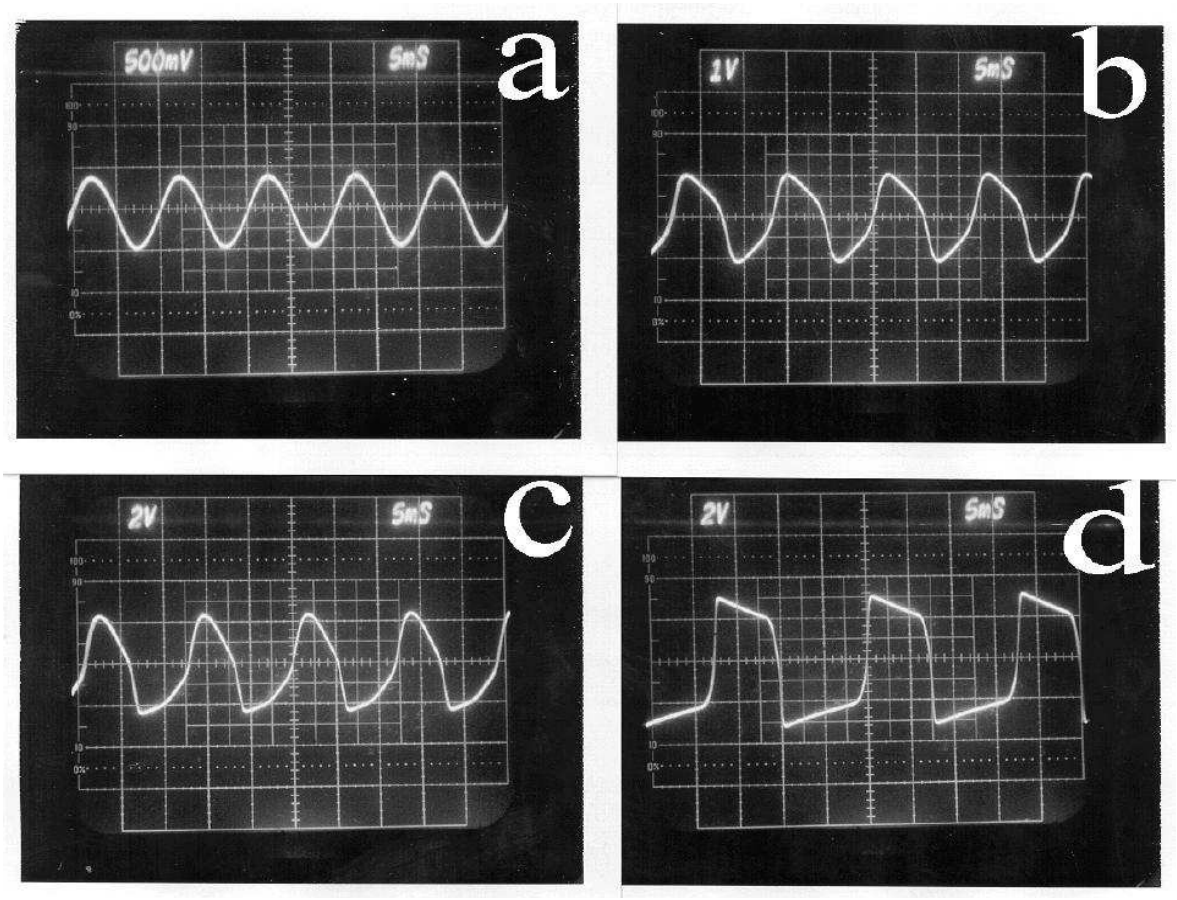

Figure 5.9: Wave forms of the limit cycle oscillator for (a) $Z_N = -100\text{K}\Omega$, (b) $Z_N = -10\text{K}\Omega$, (c) $Z_N = -5\text{K}\Omega$, and (d) $Z_N = -2.5\text{K}\Omega$. Horizontal axis is the time axis in units of $5ms$, and the vertical axis is the voltage V in units found on each of the photographs. The other parameters are $R_D = 3.5\text{K}\Omega$ and $C = 0.1\mu\text{F}$, $L = 40\text{H}$.

5.3 Single Oscillator Experiments with a time delayed feedback

We now present and discuss our first set of experiments exploring time delay effects on the oscillator characteristics. For this we just consider the single oscillator that we have described above and provide it with a self-delayed feedback mechanism. This is the experimental analog of the theoretical model studies discussed in Chapter 4, except that now we confine our experiments only to a linear feedback. To give a self delayed feedback, the output signal from the node 'V' (see Fig. 5.8) is taken through a buffer amplifier and passed onto the delay line, the output of which is connected to the node itself with a linear resistance R. The current flowing into the node through this channel is $[V(t-\tau)-V(t)]/R$

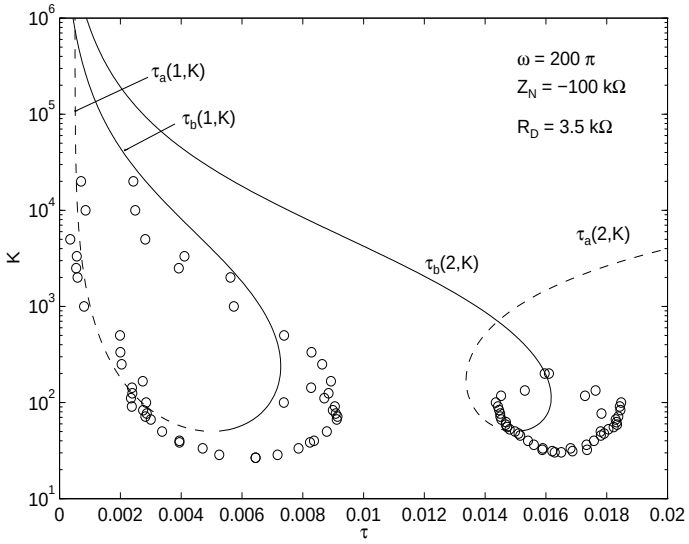

Figure 5.10: Experimental (circles) and analytical (curves drawn using Eqs. (5.14-5.15)) death islands of the oscillator with a delayed feedback. τ is millisecond.

and thus provides a self delayed-feedback.

5.3.1 Death islands

Our first objective is to study the region of amplitude death and the effect of time delay on this region of parameter space. For this we keep the oscillator's frequency and the strength of the feedback to be constant quantities and keep varying the time delay. The output voltage V of the oscillator is monitored on the oscilloscope up to the point where it shows a sudden drop in value by several orders of magnitude (i.e. nearly to zero). The value of τ is further increased till the point where the signal from the oscillator again suddenly revives to a large value. The observations are repeated for different values of the coupling strength (at the same fixed frequency) and thereby an entire parameter space in $(K - \tau)$, where amplitude death occurs, is traced out. As shown in Fig. 5.10, we obtain closed regions of parameter space where the time delayed oscillator displays cessation of oscillations. These regions are in fact the experimental manifestation of the theoretical death islands discussed earlier in the thesis. They not only resemble the islands in qualitative shape but also in a quantitative manner as we will soon demonstrate in Section 5.3.3. Note also the existence of higher order islands in accordance with the phenomena of multiple connectivity displayed by the earlier theoretical models. As was discussed in Chapter 2 (for two delay coupled oscillators) the size of the oscillator death region is a function of the frequency of the system. This can be ascertained on our single oscillator system by

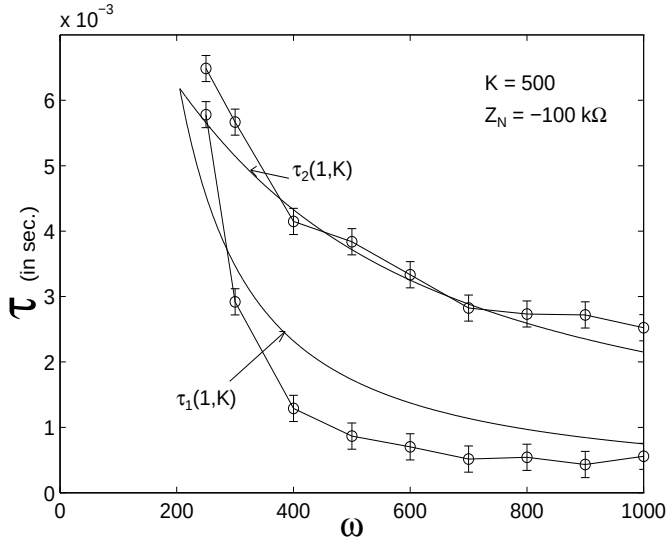

Figure 5.11: Dependence of the first death island on the intrinsic frequency at a fixed strength of feedback.

repeating the above experiment for different fixed values of the intrinsic frequency. Our results for such an experiment are shown in Fig. 5.11 where the death island regions are depicted in (ω, τ) plane.

5.3.2 Frequency suppression

Another behavior which we wish to explore is the suppression of frequencies with time delay. This result is generally observed in almost all the time delay systems; limit cycle oscillators are no exception. In the case of coupled limit cycle oscillators, it is the common frequency that is suppressed with increased time delay. Currently we demonstrate that this phenomenon exists even in our single oscillator system with a delayed feedback. We choose $K = 2 \times 10^3$ (see Fig. 5.10) and measure the time period of the output signal on the oscilloscope as the value of τ is varied. Fig. 5.12 shows the results.

5.3.3 Model equation

To provide a more quantitative understanding of our experimental results and a better analytical comparison, we develop and present in this section an approximate mathematical model of our electronic oscillator. Note that the theoretical models discussed in the previous chapters are idealized normal form models which are more convenient to analyze theoretically but may not accurately represent a specific experimental situation. A model equation for our basic limit cycle circuit (without the time delay) can be obtained as

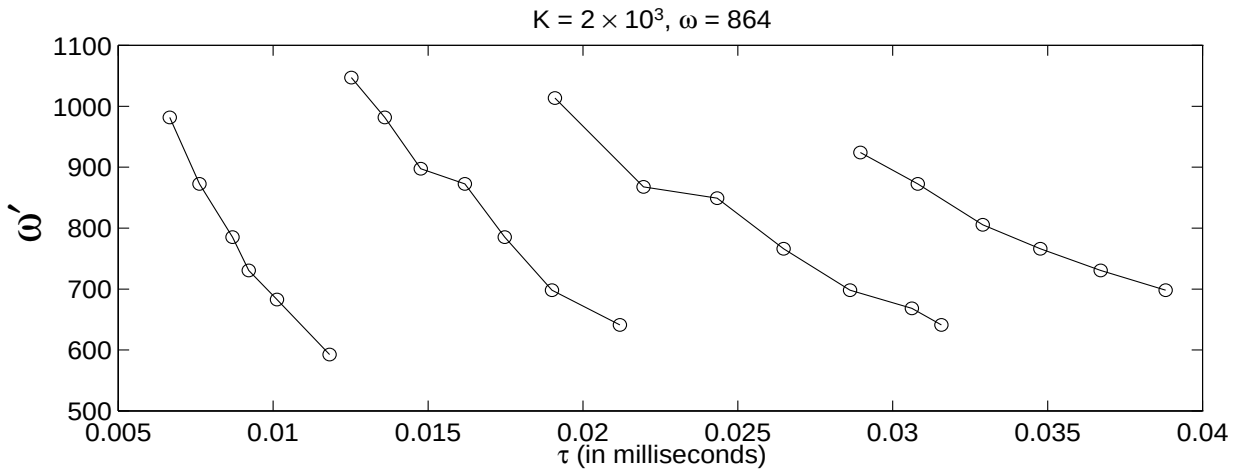

Figure 5.12: Multiple frequencies and the suppression of their magnitudes as τ is increased. $K = 2000$, $\omega = 864$.

follows. From the circuit diagram (Fig. 5.8) we note that

$$I_C + I_L + I_N = 0, \tag{5.8}$$

that is the sum of currents flowing into the node at 'V' is zero. We know that $I_C = C\dot{V}$, $I_L = \frac{1}{L}\int V dt$. (An over dot stands for the time derivative.) The expression for I_N is theoretically given by the solution of Eq. (5.3) (which is plotted as a continuous curve in Fig. 5.4(b)), and experimentally by the data points shown in that figure. The curve there is approximated by $I_N = f(V) = -a_1 V + a_3 V^3 + a_5 V^5$, where $a_1 = 0.95 \times 10^{-5}$, $a_3 = 0.22 \times 10^{-5}$, and $a_5 = 64.4 \times 10^{-5}$. Substituting these expressions for the currents into the above equation, we get

$$C\dot{V} + \frac{1}{L}\int V dt + f(V) = 0. \tag{5.9}$$

Differentiating with respect to t once and dividing through out by C yields

$$\ddot{V} + \frac{1}{LC}\int V dt + f'(V)\dot{V} = 0. \tag{5.10}$$

And substituting for $f(V)$, we obtain

$$\ddot{V} + \frac{1}{C}(-a_1 + 3a_3 V^2 + 5a_5 V^4)\ \dot{V} + \omega_0^2\ V = 0, \tag{5.11}$$

where $\omega_0^2 = 1/(LC)$. In the above approximate model equation the origin is the only fixed point, and is unstable as can be seen from the eigenvalues of the linearized equation: $\lambda = \frac{a_1}{2C} \pm \sqrt{\left(\frac{a_1}{2C}\right)^2 - \omega_0^2}$. Experimentally this means that the circuit always oscillates as long as we maintain a negative slope in the response of R_N.

When the feedback component is added we note that the current which is coming into the node at 'V' through the feedback channel is $[V(t-\tau)-V(t)]/R_K$. The current rule at the node thus becomes $I_C + I_C + I_N = [V(t-\tau)-V(t)]/R_K$. Inserting the corresponding expressions for the currents, we arrive at the following equation

$$\ddot{V} + \frac{1}{C}(-a_1 + 3a_3V^2 + 5a_5V^4)\ \dot{V} + \omega^2\ V = K[\dot{V}(t-\tau) - \dot{V}(t)], \tag{5.12}$$

where $K = 1/(R_KC)$ is the strength of feedback. (To make the feedback term just $\dot{V}(t-\tau)$, but not $\dot{V}(t-\tau) - \dot{V}(t)$ is not straight forward. But one can achieve this by a combination of circuit elements.) The stability of the origin of this equation is given by the characteristic equation which is obtained by assuming $V(t) \propto V(0)e^{\lambda t}$ and neglecting the nonlinear terms. The characteristic equation is obtained as

$$\lambda^2 + (-\frac{a_1}{C} + K)\lambda + \omega^2 = K\ e^{-\lambda\tau}. \tag{5.13}$$

By following the method outlined in the previous chapters, we look for the regions where the combined system's oscillations are suppressed. These regions are given by the conditions that $\tau_a(n,K) < \tau_b(n,K)\ \ n = 1, 2, \ldots$, where the curves are defined by

$$\tau_a(n,K) = \frac{2(n-1)\pi + \cos^{-1}(1 - \frac{a_1}{CK})}{-\frac{A}{2} + \sqrt{(\frac{A}{2})^2 + \omega^2}}, \tag{5.14}$$

$$\tau_b(n,K) = \frac{2n\pi - \cos^{-1}(1 - \frac{a_1}{CK})}{\frac{A}{2} + \sqrt{(\frac{A}{2})^2 + \omega^2}}, \tag{5.15}$$

where $A = \sqrt{\frac{2a_1}{C}K - (\frac{a_1}{C})^2}$, and $n = 1, 2, \ldots$. As we noted already, there are two eigenvalues with positive real parts (i.e. in the left hand side of the complex eigenvalue plane) in the absence of time delay. So any closed death island region should now be bounded on one of the sides by a curve across which the eigenvalue pair crosses into the right half plane. The other side of the bounded region must be the curve across which the eigenvalues make a transition to the left half plane. By evaluating the derivatives with respect to τ of the eigenvalues, and examining them across the above two curves, we can come to the following conclusion:

$$Re\left(\frac{d\lambda}{d\tau}\right)\Big|_{Re(\lambda)=0} \begin{cases} < 0 & \text{on } \tau_a, \\ > 0 & \text{on } \tau_b. \end{cases} \tag{5.16}$$

Accordingly along the τ-axis, the curve τ_a should be on the left side boundary of the death islands and τ_b should be the right side boundary. However the occurrence of the death island depends on the ordering of these curves. We refer to Chapter 2 for further discussion on the ordering of the curves. In Fig. 5.10 we plot the analytical curves discussed above

as solid lines. The experimental points are shown as open circles. We notice that the experimental results are quite close to the analytic estimates. The slight discrepancies from the analytic curves can be attributed to experimental errors as well as the inaccuracy of the theoretical model itself (for example in the modeling of the nonlinear resistance). The experimental errors can arise from a combination of the in-built tolerances of the various components used and the effect of one on the other as well as measurement errors. The mismatch between the experimental data and analytic estimates appears most for larger values of K. This is understandable since at these strengths of feedback, the current that is flowing into the oscillator due to feedback is very high compared to its internal currents. This obviously leads to erroneous behavior of the components.

5.4 Experiments on Two delay coupled Limit Cycle Oscillators

We now proceed with our principal experiment, namely the study of two limit cycle oscillators that are linearly coupled with a time delay. Such a system of coupled oscillators can exist in four possible states: (i) an in-phase locked state in which the two oscillators are synchronized at the same phase and frequency (ii) an anti-phase locked state in which they oscillate with the same frequency but are 180 degrees out of phase , (iii) an oscillator death state in which they do not oscillate, and (iv) a phase drift state in which each oscillator oscillates at its own frequency and their mutual phases drift through 2π . The last state is not a coherent collective state and we are not interested in its dynamics. We will study the effect of time delay on the first three states. We further restrict ourselves to two identical oscillators so that the frequencies are the same for both the oscillators. We begin by briefly describing the electronic circuitry for this system and then present its experimental response in these three regions. Then an experiment is carried out to determine the boundaries of the oscillator death region. We also measure the frequencies both in the in-phase and the anti-phase states as τ is increased to study frequency suppression. Finally we present a mathematical model and compare our experimental results with the analytic results obtained from its solution.

5.4.1 Circuit design

The coupling of the two oscillators is done as shown in Fig. 5.13. The components of the two oscillators are suffixed by 1 and 2 respectively. The coupling to the first oscillator is

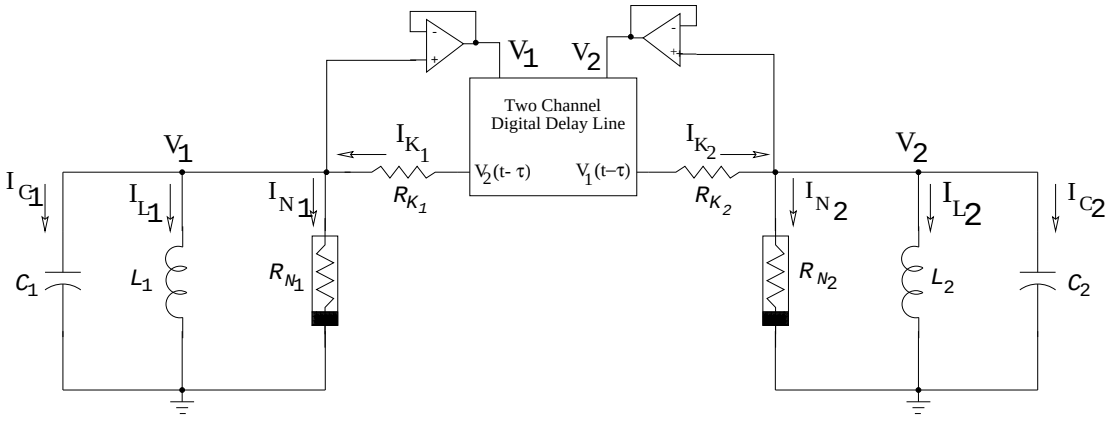

Figure 5.13: Two coupled limit cycle oscillators with time delay. In the experiment, both are identical with the same component values and a finite time delay. The parameters are $C_1 = C_2 = 0.1\mu$F, $L_1 = L_2 = 200/\pi^2$, R_{N_1} and R_{N_2}) have (identical) voltage-current response given in Fig. 5.4.

through the resistance R_{K_1} and that to the second oscillator is through R_{K_2}. The currents flowing in R_{K_1} and R_{K_2} are I_{K_1} and I_{K_2} respectively, where

$$I_{K_1} = \frac{1}{R_{K_1}}[V_2(t-\tau) - V_1(t)], \qquad I_{K_2} = \frac{1}{R_{K_2}}[V_1(t-\tau) - V_2(t)]. \tag{5.17}$$

So the coupling is linear, and is inversely proportional to the resistances R_{K_1} and R_{K_2}. The branches coming out of the nonlinear resistances and leading to the input of the delay line do not carry any current because of the infinite input impedances provided by the OP-AMPs shown. Since our interest at the moment is on identical oscillators, we make both the oscillators oscillate with the same frequencies. We also make the amplitudes of both the oscillators identical. The component values chosen are the same as those for the single oscillator discussed in the previous section (see Fig. 5.8): Each oscillator's frequency is 100 cycles/sec. Time delay is varied in milliseconds and the resistances (which are inversely proportional to the coupling strengths) are varied from a few tens of Ω to a few MΩ.

5.4.2 Experimental Results

We maintain the frequencies of the two oscillators identical by varying the inductance values. Coupling strength is made identical by choosing the same coupling resistances. Now as we vary τ, we examine the output of both the signals on the oscilloscope. In the phase locked state the waveforms from both the channels can be stabilized on the oscilloscope because they can be triggered at the same time. This is also one test to check

the oscillators for their identical frequencies. In the in-phase locked state the waveforms can be stabilized with a zero phase difference. As τ is increased the system goes to a zero amplitude state and emerges into a phase locked state. The value of Z_N is fixed at $-100\text{K}\Omega$, $R_D = 3.5\text{K}\Omega$. In Fig. 5.14, the three main kinds of behavior of in-phase locking (for $\tau = 0.514$ ms), death (for $\tau = 2$ ms) and anti-phase locking (for $\tau = 4.428$ ms) are displayed.

Now we perform an experiment to determine the oscillator death state and then study the phase locked states. Following the same procedure described earlier to find the boundaries of oscillator death, we determine now this region where the oscillations of both the oscillators are suppressed at the same time. The values of Z_N and R_D are the same as mentioned above. Since the oscillators are identical in their functioning and the coupling is also symmetric, this steady state is shown by both the oscillators uniformly. (That is they go to the death state collectively.) The results are shown in Fig. 5.15(a). The region forms a closed island and further increases of τ will have no death for this particular choice of the parameters. The dependence of the width of the death island on the common initial frequency ω is shown in Fig. 5.15(b). As we have already noted, the two identical oscillators now can acquire two kinds of periodic collective states: (i) in-phase locked solution, (ii) anti-phase locked solution. We choose $K = 500$ (corresponding $R_K = 20\text{K}\Omega$), $\omega = 200\pi$. The period of the collective oscillation of the two oscillators is observed on the oscilloscope screen and the period is noted down as the value of τ is varied. In Fig. 5.16, we show the experimental results. The lines just connect the experimental points. In the experiment, the oscillations are seen as both in-phase (stars in the figure) and anti-phase (circles in the figure) oscillations, which respectively correspond to phase locking with zero phase difference and a phase difference of π. There are regions with multiple stable solutions. These can be obtained by giving a perturbation to the circuit in the form of, for example, introducing a noisy connection at one of the capacitors. By a slow and steady variation of τ the oscillators can continue to exist in a particular state either in-phase or anti-phase. In the region where there are both these states stable, a perturbation can alter the state to which the system locks. In the following section we give a set of model equations for the circuit diagram and compare the results with the experiment.

5.4.3 Model equations

Now we provide a set of two model equations to describe the circuit shown in Fig. 5.13. Before suppressing the suffixes on the symbols (to treat them as identical), we write below the two equations governing the two oscillators if they were non identical. However, we may assume that the nonlinear response of the resistances R_{N_1} and R_{N_2} are the same.

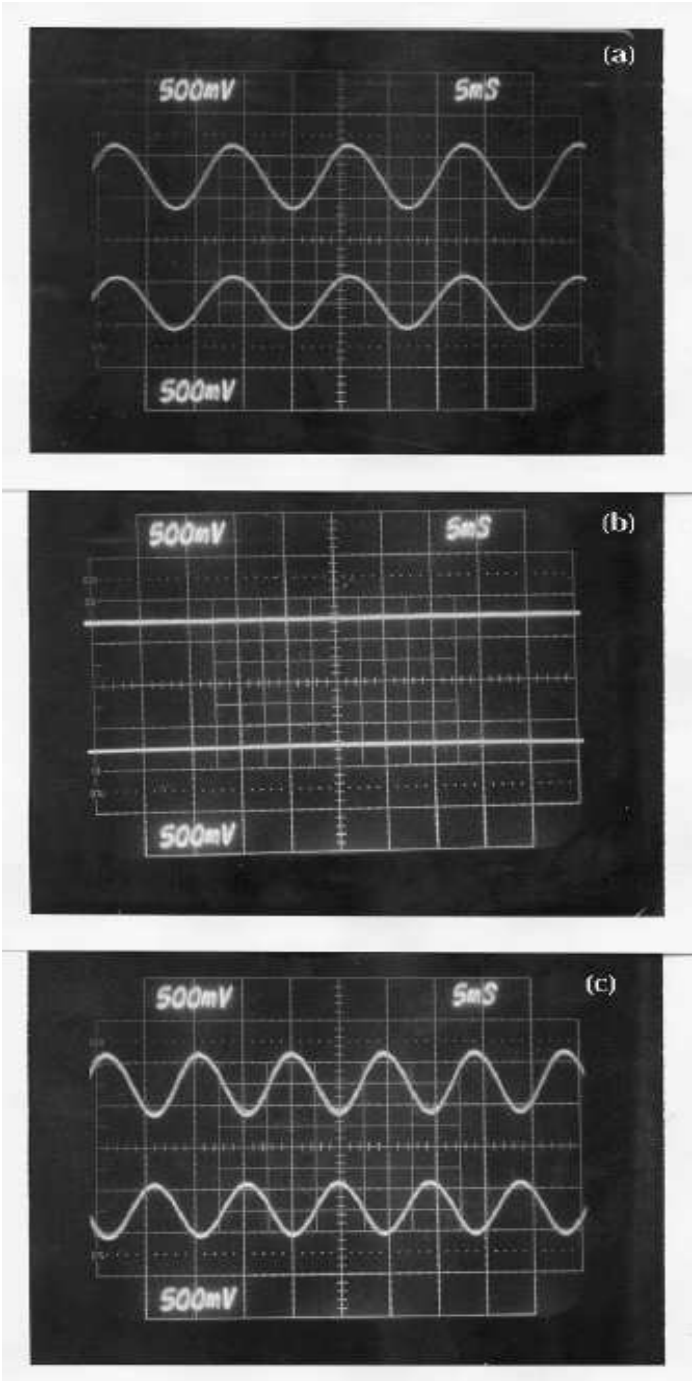

Figure 5.14: The behavior of two delay coupled oscillators plotted in time. The vertical axis is the voltage of each of the oscillators. The horizontal axis is the time in units of 5 ms. (a) in-phase locking for $\tau = 0.514$, (b) amplitude death for $\tau = 2$ ms, and (c) anti-phase locking for $\tau = 4.428$ ms. The other parameters are $Z_N = -100\text{K}\Omega$ and $R_D = 3.5\text{K}\Omega$.

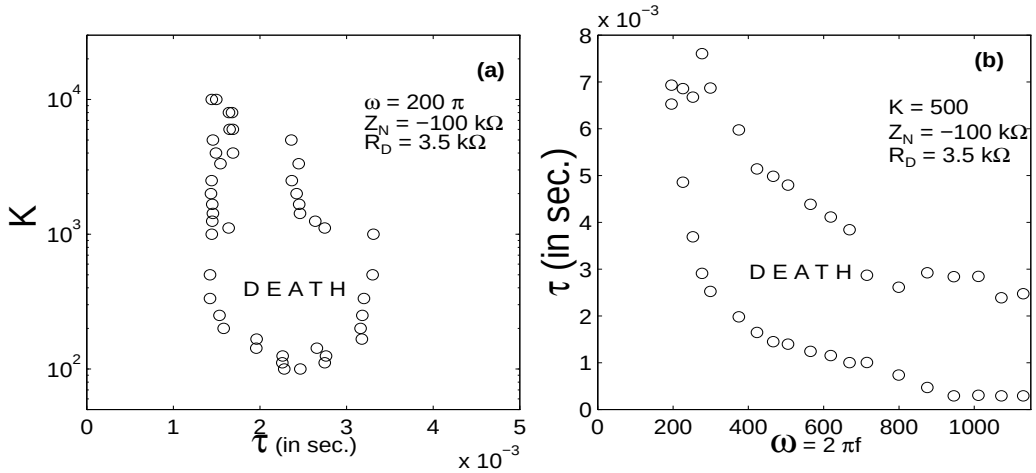

Figure 5.15: (a) Experimentally obtained death island. (b) The cross section of the death island as a function of ω. The parameters are as shown in Fig. 5.13.

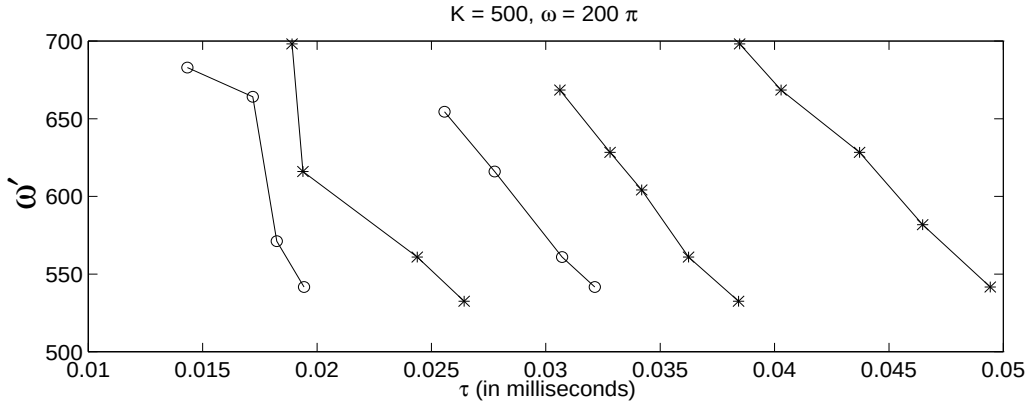

Figure 5.16: Multiple frequencies and the suppression of their magnitudes as τ is increased. The data points with stars ($\star$) correspond to in-phase solutions and those with circles ($\circ$) to anti-phase solutions. $K = 500$, $\omega = 200\pi$.

The equations are written from the current sum rule which says that the sum of currents flowing into a node [here I_{K_1} (respectively I_{K_2})] is equal to the sum of currents flowing out of the node [$I_{C_1} + I_{L_1} + I_{N_1}$ (respectively $I_{C_1} + I_{L_1} + I_{N_1}$)]. Using the same expressions for the currents as before, differentiating the resultant equations, and dividing each equation by the corresponding capacitances that appear in that equation, the following equations can be written down:

$$\ddot{V_1} + \frac{1}{C_1}(-a_1 + 3a_3V_1^2 + 5a_5V_1^4)\ \dot{V}_1 + \omega_1^2\ V_1 = K_1(\dot{V}_2(t-\tau) - \dot{V}_1(t)), \tag{5.18}$$

$$\ddot{V_2} + \frac{1}{C_2}(-a_1 + 3a_3V_2^2 + 5a_5V_2^4)\ \dot{V}_2 + \omega_2^2\ V_1 = K_2(\dot{V}_1(t-\tau) - \dot{V}_2(t)), \tag{5.19}$$

where the frequencies are $\omega_j = \frac{1}{\sqrt{L_jC_j}}$, and the coupling strengths $K_j = \frac{1}{C_jR_{K_j}}$, $j = 1, 2$. From now on, since our interest currently is on identical oscillators with identical coupling, we suppress the indices 1 and 2 on all the components. Due to the finite time delay τ, V_1 and V_2 remain distinct. We now derive the boundaries of the death region for this model by linearizing about the zero equilibrium state and finding curves across which the eigenvalues transit to the right hand side of the complex eigenvalue plane. This is done by assuming that $V_{1,2}(t) \propto V_{1,2}(0)e^{\lambda t}$, and substituting these in Eqs. (5.18-5.19) and discarding the nonlinear terms. This gives the following characteristic equation:

$$\lambda^2(\lambda - \frac{a_1}{C} + K)^2 + 2\omega^2(\lambda - \frac{a_1}{C} + K)\lambda + \omega^4 - K^2\lambda^2e^{-2\lambda\tau} = 0, \tag{5.20}$$

or by taking the last term to the right hand side and taking a square root, the following two equations are obtained.

$$\lambda^2 + (-\frac{a_1}{C} + K)\lambda + \omega^2 = \pm K\ e^{-\lambda\tau}. \tag{5.21}$$

The only difference between this and that obtained from (Eq. 5.13) for a delayed feedback oscillator is the emergence of $\pm$ sign on the right hand side. We summarize the analysis by noting that this $\pm$ sign will parameterize the curves (Eqs. (5.14-5.15)) with $n\pi$ rather than $2n\pi$. The curves thus are given by

$$\tau_1(n, K) = \frac{(n-1)\pi + \cos^{-1}(1 - \frac{a_1}{CK})}{-\frac{A}{2} + \sqrt{(\frac{A}{2})^2 + \omega^2}}, \tag{5.22}$$

$$\tau_2(n, K) = \frac{n\pi - \cos^{-1}(1 - \frac{a_1}{CK})}{\frac{A}{2} + \sqrt{(\frac{A}{2})^2 + \omega^2}}, \tag{5.23}$$

where $A = \sqrt{\frac{2a_1}{C}K - (\frac{a_1}{C})^2}$, and $n = 1, 2, \ldots$. The eigenvalues behave across these curves in the same way as for the similar curves in the previous section. In particular the relations (5.16) hold with the suffixes a and b replaced by 1 and 2 respectively. In Fig. 5.17 we

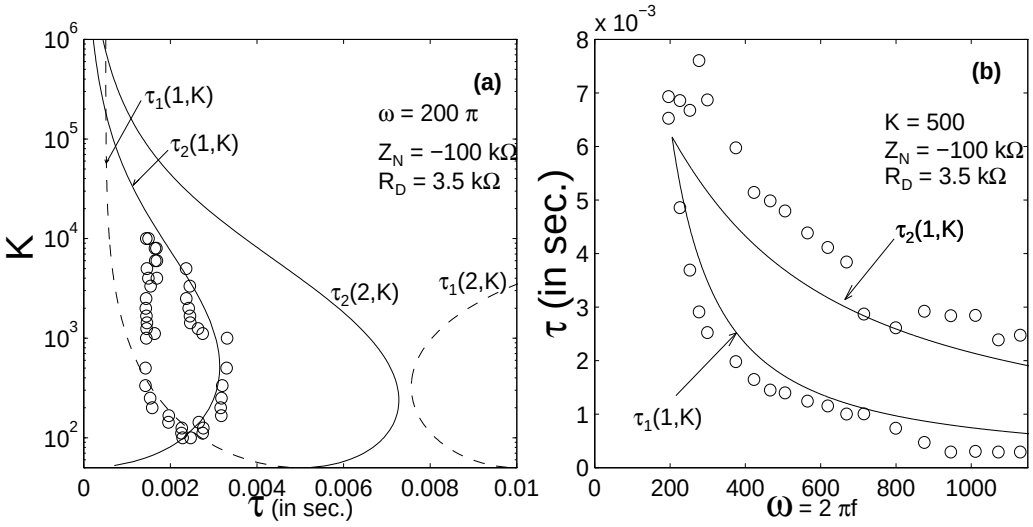

Figure 5.17: Analytical boundaries of the death regions (a) The death islands in (K, τ) space. (b) The dependence of width of the death island region on τ at $K = 500$. The experimental data shown in circles is the same as that displayed in Fig. 5.15

show these curves for $n = 1, 2$ along with the experimentally found values representing the boundaries of the death islands. For the current set of values of the parameters, there is only one death island.

The match is quite satisfactory for weaker couplings. As the coupling gets stronger the mismatch between the theoretical curves and the experimental points becomes more. This is similar to what we had faced in the last section (see Fig. 5.10) for large coupling strengths. The error is also due to the fact that, in the experiment, the two oscillators that are constructed cannot be made to oscillate exactly with identical frequencies to the accuracy of decimal places. Another possible error is also due to the small current that passes through the input arms of the OP-AMPs in the figure. Suppose this current is proportional to the voltage at the corresponding node in a linear fashion. This factor would essentially reduce the value of a_1. A reduced value of a_1 will bring the height of the death island substantially, as can also be seen by plotting the the Eqs. (5.22-5.23).

In Fig. 5.17(a), we see that there is only one region of amplitude death. The amplitude death region however may not occur if the frequency of oscillation itself is below a certain threshold. That is the size of the death island is diminished with decreasing value of the common frequency and vanishes below a threshold just as the case in the previous section (see Fig. 5.11). For $K = 500$, which results in a finite span of death region along the τ-axis,

the plot in Fig. 5.17(b) shows the region of death island (plotted from Eqs. (5.22-5.23)).

5.5 Summary and Discussion

In this Chapter, we have presented experimental results of investigations carried out on electronically constructed limit cycle oscillators in the presence of a time delay element. Two sets of experiments have been done - one for a single oscillator and another for two coupled oscillators. In the single oscillator experiment time delay is introduced in the form of a linear feedback term. For the coupled oscillators time delay appears in the mutual linear coupling. Both sets of experiments demonstrate the stabilizing influence of time delay (inducing quiescent or death states), the creation of multiple frequency states and the time delay induced suppression of the collective frequency. The existence of death islands for identical oscillators, an important theoretical result, is clearly validated by these experiments - perhaps for the first time. The experimental results also agree reasonably well with quantitative estimates obtained from approximate theoretical models of the electronic circuits. The discrepancies can be largely attributed to experimental sources of error which are not reflected in the idealized mathematical models of the circuits. We briefly discuss below some of these potential sources of error which need to be recognized particularly if one plans to carry out such experiments on a system of large number of oscillators.

The sources of experimental error can be broadly divided into three categories : (i) error of the electronic components (e.g, tolerance), (ii) error of the electronic blocks (e.g. limitations of currents beyond a certain threshold), (iii) errors in measurements (e.g. reading an analog oscilloscope, which is used in the current experiments, is not absolutely accurate; reading the values of resistances using a multimeter in different modes). Type (i) errors are probably the least important for our experiments - particularly in the case of the single oscillator experiment. They play some role in the case of the two oscillator case where although the same components were chosen, differences in frequencies arose because of the tolerances of the components. And finally, the amplitudes were also slightly different because the OP-AMPs were found to be not identical in operation. Since the main focus on the death islands was to study the identical oscillators, the inductance value of one of the oscillators was slightly shifted than what is reported to make both the oscillators acquire identical frequencies. This can be a source for some discrepancy between the model and the actual experiment. Type (ii) errors appear to have been important in the regime of strong coupling constants (e.g. as found in Fig. (5.17)). Large

values of coupling constants imply that we must use small values of resistance to couple the oscillators. Theoretically, as the resistance goes to 'zero', the currents go to '∞' and so do the coupling strengths. Needless to say, there are no infinite currents in any experiment. So we are bound to face errors at large values of coupling strengths mainly because of the limitations of the electronic blocks. Finally, another potential source of error is associated with the digital delay line. Ideally it should not induce any extraneous behavior of its own. In the present experiments, some difficulty was faced due to the time delay element when the delays required were significantly smaller than one millisecond. The current time delay circuit cannot, by its intrinsic limitations, handle higher frequencies, say those of the order of kilo cycles/sec. and tends to give rise to chaotic signals. We have found it best to avoid that regime.

Bibliography

[1] A. A. Brailove and P. S. Linsay. An experimental study of a population of relaxation oscillators with a phase-repelling mean-field coupling. *Int. J. Bif. Chaos*, 6:1211–1253, 1996.

[2] G. P. King and S. T. Gaito. Bistable chaos. I. Unfolding the cusp. *Phys. Rev. A*, 46:3092–3099, 1992.

[3] M. G. M. Gomes and G. P. King. Bistable chaos. II. Bifurcation analysis. *Phys. Rev. A*, 46:3100–3110, 1992.

[4] Yao-Huang Kao and Ching-Sheu Wang. Analog study of bifurcation structures in a van der pol oscillator with a nonlinear restoring force. *Phys. Rev. E*, 48:2514–2520, 1993.

[5] M. Lakshmanan and K. Murali. *Chaos in nonlinear oscillators – controlling and synchronization*. Nonlinear Science Series A Vol. 13. Wold Scientific, 1996.

[6] J. Kawata, Y. Nishio, and A. Ushida. Analysis of Chua's circuit with transmission line. *IEEE Trans. Circ. Syst. -I: Fund. Theor. Appl.*, 44:556–558, 1997.

[7] P. Ash. Attractors of randomly forced electronic oscillator. *Physica D*, 125:302–310, 1999.

[8] Sergio Franco. *Design with Operational Amplifiers and Analog Integrated Circuits*. McGraw-Hill Book Company, Singapore, Singapore, 1998.

[9] Jǐrí Dostál. *Operational Amplifiers*. Butterworth-Heinemann, Boston, 2nd edition, 1993.

[10] J. G. Graeme, G. E. Tobey, and L. P. Huelsman Eds. *Operational Amplifiers – Design and Applications*. McGraw-Hill Book Company, New York, 1971.